Control System Development for LoCO AUV

A Thesis

SUBMITTED TO THE FACULTY OF THE

UNIVERSITY OF MINNESOTA

BY

Kimberly Barthelemy

IN PARTIAL FULFILLMENT OF THE REQUIREMENTS

FOR THE DEGREE OF

Bachelor of Aerospace Engineering and Mechanics

With Honors

Faculty Adviser: Professor Junaed Sattar, PhD

May 2021

Copyright Page

Acknowledgements

I would like to thank my supervisor Professor Junaed Sattar for welcoming me into the Interactive Robotics and Vision Lab and for providing me the opportunity to participate in undergraduate research. I appreciate the wide variety of topics I have been able to explore and for the hands on experience working with robots in the field. I would also like to thank Michael Fulton for answering the endless questions and being a mentor to many of us undergraduates as we take our first steps into the field of robotics.

Additionally, thank you to Professor Yohannes Ketema and Professor Ryan Caverly for being on the reviewing honors committee for this thesis. The feedback and support I have received in my pursual of this thesis has been very much appreciated.

Abstract

The goal of this thesis is to design an automatic control system capable of autonomous navigation and minimal human interaction when provided with a defined path for the University of Minnesota's homebuilt autonomous underwater vehicle (AUV), LoCO. This thesis examines the mathematical modeling of rigid, underwater, 6 DOF vehicles in relation to Earth's inertial frame by equating the thrusting forces and moments provided by the vehicle's control system to the hydrodynamic forces and moments acting against the vehicle's motion as it travels through a body of water. Further, the derived 6 DOF equations are simplified to two systems of 3 DOF equations that more accurately represent the LoCO AUV's capabilities in the horizontal plane and vertical *xz*-plane. The simplified two systems of 3 DOF equations are then linearized about a specific forward velocity and the stability of each system is examined in detail before being transformed into a transfer function which can be used directly for control system design. In regard to control system design, critical design characteristics such as steady state error, settling time, rise time, and maximum overshoot are discussed, along with the fundamentals of PID control.

Based on the performance requirements of the LoCO platform, separate PI and PID control systems are designed and analyzed for use as LoCO's first control system.

Table of Contents

List of Tables

List of Figures

Chapter 1

Introduction

Autonomous underwater vehicles (AUVs) and remotely operated vehicles (ROVs) are critical tools in the modern industrial and scientific worlds when it comes to working in marine and aquatic environments. As the names suggest, AUVs operate independently of humans, while ROVs are tethered to and controlled by a ship or ground station to perform operations nearby [1]. ROVs have the advantage of sending data directly to the station manning them and can be monitored more easily for any faults that occur during operation but have to remain close to their source and tend to be slower moving. AUVs have the advantage of being able to travel long distances quickly and collect a huge array of data independently before having to return to a known location where the data can be analyzed and the AUV can be prepared for its next deployment. Due to their increased autonomy, they are also able to travel into smaller areas where it may be unsafe for human divers. The downside of AUVs is that their data cannot be transmitted in real time and it can be more difficult to monitor any faults that occur during operation.

AUVs have been used to study predatory behavior in sharks [2], for mine reconnaissance [3], to collect bathymetric data of certain bodies of water [4], and perform underwater pipeline detection in areas where these systems are failing [5]. In the oil and gas field specifically, AUVs have proven to be more efficient in the long term [6] compared with ROVs and human divers, but tend to have a higher cost of entry due to the

necessary design robustness. Part of the robustness that makes these vehicles so expensive is their control systems. In order to have a fully functional AUV it is critical that the control system provides stability and maneuverability, as well as fully autonomous navigation independent of human oversight.

1.1. Control Background

Control systems are used whenever it is desirable to have a system behave in a certain way. Things like temperature, speed, altitude, and electrical impulses in biological systems are all examples of where control systems have been used. In order to design a control system, an understanding of the dynamic system of interest has to be obtained. Some of the simpler systems like temperature control in a house only require basic control systems that turn off or on if a certain threshold is gone above or below. More complex control systems may need to meet stringent performance requirements, may have to change as the dynamics of the system changes, or have multiple embedded control systems in order to assert an overall higher level of control over the dynamic system.

There has been extensive work on trajectory tracking both for terrestrial and aquatic vehicles. Trajectory tracking controls range from simplistic PID controllers to more advanced adaptive controls. A survey on AUV control design up to the year 2000 was performed by Yuh [7] that found sliding controllers, nonlinear controllers, adaptive controllers, neutral network controllers, and fuzzy controllers had been implemented. While not an exhaustive list of complex trajectory tracking controllers, each of these have the ability to self-tune, allowing the AUV to compensate for changes in vehicle dynamics.

Comparative studies between controllers have also been done. One study performed by Lea et al. [8] implemented PID, fuzzy logic, and sliding mode controllers on an AUV to compare the performance and complexity between the three different speed controllers. The PID controller was found to be the simplest one but took a comparatively long time to respond since the AUV system is a nonlinear one. The fuzzy logic and sliding mode controllers performed better, but required additional tuning and system modeling, both of which are time consuming and may be difficult to implement correctly depending on one's knowledge of control systems. The conclusion was that no controller was optimal and would depend heavily on user preference.

In many of the comparative studies basic controllers are first designed and the more complex controllers are built up to as more experience is gained and knowledge of the system and its performance is learned. For some AUV systems that operate as diver companions or operate autonomously for short periods of time, a simple PID control system may be sufficient. For AUV systems that need to be able to reliably perform alone or have extreme stability an adaptive controller will likely perform more desirably. In some cases, this level of complexity can be worked up to as systems become more complex and more is expected out of them. As in the case of Aqua AUV, a finned hexapod robot, many control systems were created and built upon before the current version was put into place.

1.2. The LoCO AUV

The Interactive Robotics and Vision Laboratory at the University of Minnesota Twin Cities has designed, prototyped, and released LoCO AUV, a **Lo**w **C**ost **O**pen, Autonomous Underwater Vehicle over the course of the past couple of years [9]. LoCO is

designed to be easily built, transported, and deployed by a single person, with the parts being primarily off-the-shelf and additively manufactured. While LoCO does not have all the capabilities of the more expensive AUVs, it has a wide range of capabilities for its price point and is constantly undergoing further development to widen its use cases.

LoCO is composed of two watertight enclosures that house its computing and power systems, as well as all electronics and a variety of sensors. It moves via a three propellor system, two of which are behind the enclosures and one of which is in between the enclosures as seen in Figure 1. Many of the structural components are 3D printed which lends the AUV well to modularity and customization. To give a feeling for its size, LoCO is approximately 73.1 cm long, 34.4 cm wide, 14.1 cm tall, and weighs approximately 27 pounds. It has a maximum operational velocity of 1.5 meters per second. On board are two cameras for imaging and video, a Jetson TX2 capable of deep learning, a Raspberry Pi 4 that handles control, an inertial measurement unit (IMU) for the autopilot, an LED screen for human-robot interaction, and a pressure sensor that enables depth measurements to be made. Altogether these sensors and systems provide a fairly wide array of capabilities for such a low-cost AUV.

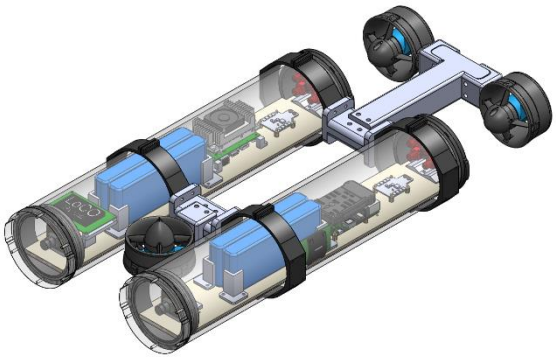

Figure 1: *Isometric View of LoCO AUV*

Since its creation, LoCO has successfully undergone field trials in pools, lakes, and the ocean. Over its development LoCO has been controlled by teleoperation over ethernet and has used visual commands to perform preprogrammed movement algorithms. Using a tether can be burdensome, especially when it comes to field trials

since the tether required to run from LoCO to a ground station limits the range of the AUV and requires another individual for operation to ensure the tether does not become tangled. LoCO operated with no tether to a ground station for the first time in the winter of 2019 when the piloting system became advanced enough to execute preprogrammed command algorithms based on gestural input or AR tags. In order to give LoCO the full range of autonomy it was designed for, an automatic control system must be created that is capable of autonomous navigation and minimal human interaction when provided with a defined path [10], [11].

1.3. Thesis Organization

The goal of this thesis is to design an automatic control system capable of autonomous navigation and minimal human interaction when provided with a defined path. The second chapter reviews the equations of motion for a 6 degree of freedom (DOF) underwater vehicle. Chapter three provides simplified, linearized 3 DOF systems of equations specific to LoCO AUV and determines the transfer functions of these systems necessary for control system design. Chapter four designs the control system, selects all necessary gains, and investigates the validity of the selected system. Finally, chapter five reviews that which is learned during the design of the control system and provides recommendations for future work.

Chapter 2

Mathematical Modeling of Underwater Vehicle

The first step in creating a control system is understanding the dynamic model for which the system is being built. The derivations for the generalized equations of motion for underwater vehicles are derived completely by Fossen [12] and Wadoo et al. [13]. Also critical to the understanding of the linearization discussed herein is Gonzalez [14]. The author recommends the further consideration of Fossen's works for anyone who is looking for a more detailed derivation of the full set of dynamic equations or if unfamiliar with the general field of dynamics.

2.1. Kinematics and Reference Frames

All marine vehicles are 6 degree of freedom (DOF) systems since they require 6 measures to completely define their position and orientation. The first 3 of these measures define the AUV's axial position and the last 3 define the AUV's angular orientation. There exists a standard terminology used when discussing these 6 measures. Displacement in the *x*-direction is called "surge", displacement in the *y*-direction is called "sway", and displacement in the *z*-direction is called "heave". Likewise, rotation about the *x*-axis is called "roll", rotation about the *y*-axis is called "pitch", and rotation about the *z*-axis is called "yaw".

Critical to the discussion and derivation of the rigid body 6 DOF set of equations is the discussion of reference frames. It is best to frame the problem using two sets of reference frames. The first reference frame called the "body frame" is attached to the AUV. The second reference frame called the "NED frame" is attached to the Earth and is

an inertial frame. Though different frames for Earth are sometimes used, the NED frame sets the three frame axes along the North, East, and down directions, where down points towards the Earth's core. This is fairly standard for naval and aerospace applications.

As suggested, the *x*-axis of the NED frame points North relative to the Earth, the *y*-axis points East relative to the Earth, and the *z*-axis points towards the Earth's center. In the Earth frame, this means that rotation about the *x*-axis or Northern axis correlates with roll, rotation about the *y*-axis or Eastern axis correlates with pitch, and rotation about the *z*-axis or downward pointing axis correlates with yaw. The body frame attached to the AUV is attached at the center of buoyancy of the vehicle. The *x*-axis of the body frame points out the bow of the vehicle, the *y*-axis of the body frame points out the starboard side of the vehicle, and the *z*-axis points downwards underneath the vehicle. The relative positions of the frames, as well as the corresponding velocities and forces can be seen in Figure 2.

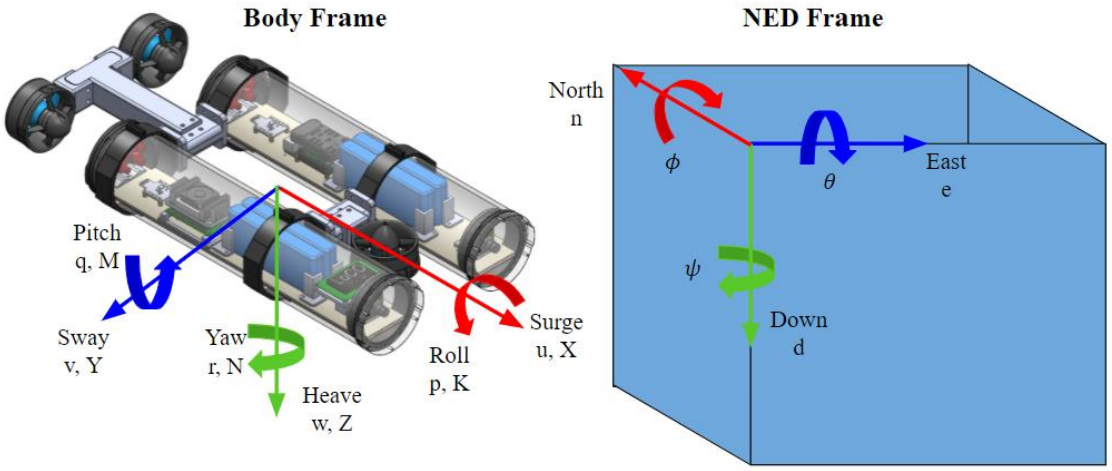

Figure 2: *Body Frame and NED Frame*

The positions, angles, velocities, forces, and moments are defined by the Society of Naval Architects and Marine Engineers (SNAME) [15] as:

$$\text{NED position: } \boldsymbol{p}^n = \begin{bmatrix} n \\ e \\ d \end{bmatrix} \tag{1a}$$

$$\text{Euler Angles: } \boldsymbol{\Theta} = \begin{bmatrix} \phi \\ \theta \\ \psi \end{bmatrix} \tag{1b}$$

$$\text{Body frame linear velocity: } \boldsymbol{v}^b = \begin{bmatrix} u \\ v \\ w \end{bmatrix} \tag{1c}$$

$$\text{Body frame angular velocity: } \boldsymbol{\omega}^b = \begin{bmatrix} p \\ q \\ r \end{bmatrix} \tag{1d}$$

$$\text{Body frame force: } \boldsymbol{f}^b = \begin{bmatrix} X \\ Y \\ Z \end{bmatrix} \tag{1e}$$

$$\text{Body frame moment: } \boldsymbol{m}^b = \begin{bmatrix} K \\ M \\ N \end{bmatrix} \tag{1f}$$

The generalized motion of an AUV in 6 DOF can be described the following 3 vectors, composed of the 6 SNAME definitions above.

$$\boldsymbol{\eta} = \begin{bmatrix} \boldsymbol{p}^n \\ \boldsymbol{\Theta} \end{bmatrix} = \begin{bmatrix} n \\ e \\ d \\ \phi \\ \theta \\ \psi \end{bmatrix}, \qquad \boldsymbol{\nu} = \begin{bmatrix} \boldsymbol{v}^b \\ \boldsymbol{\omega}^b \end{bmatrix} = \begin{bmatrix} u \\ v \\ w \\ p \\ q \\ r \end{bmatrix}, \qquad \boldsymbol{\tau} = \begin{bmatrix} \boldsymbol{f}^b \\ \boldsymbol{m}^b \end{bmatrix} = \begin{bmatrix} X \\ Y \\ Z \\ K \\ M \\ N \end{bmatrix} \tag{2}$$

Both the NED and body frame can be seen pictured in Figure 2 with the SNAME defined elements and terminology attached to the respective axes.

2.2. Converting from Between Body and NED Frame

To go in between the body and NED frames a rotation matrix $\boldsymbol{R}$ is used. This matrix is made up of operations on the Euler angles derived from the standard Euler "3-2-1" method. To go from the body frame to the NED frame, the rotation matrix is:

$$\boldsymbol{R}_b^n(\boldsymbol{\Theta}) = \begin{bmatrix} c\psi c\theta & -s\psi c\phi + c\psi s\theta s\phi & s\psi s\phi + c\psi c\phi s\theta \\ s\psi c\theta & c\psi c\phi + s\phi s\theta s\psi & -c\psi s\phi + s\theta s\psi c\phi \\ -s\theta & c\theta s\phi & c\theta c\phi \end{bmatrix} \tag{3}$$

where the subscript represents the body frame and the superscript represents the NED frame, together indicating that this is the matrix that takes one from the body frame to the NED frame. The shorthand used with the angles is $s = \sin(\cdot)$ and $c = \cos(\cdot)$. Since the rotation matrix is orthogonal the inverse rotation is simply $\boldsymbol{R}^{-1} = \boldsymbol{R}^T$.

2.3. Rigid 6-Degrees of Freedom Body Equations of Motion

The 6 DOF nonlinear dynamic equations of motion is a function of the forces and moments that make up the accelerations experienced by the body. In the body frame and as a function of velocity, Fossen [12] provides the equation:

$$\boldsymbol{M}\dot{\boldsymbol{\nu}} + \boldsymbol{C}(\boldsymbol{\nu})\boldsymbol{\nu} + \boldsymbol{D}(\boldsymbol{\nu})\boldsymbol{\nu} + \boldsymbol{g}(\boldsymbol{\eta}) = \boldsymbol{\tau} + \boldsymbol{g_0} + \boldsymbol{w} \tag{4}$$

where $\boldsymbol{M}$ is the inertial matrix of the system that includes the added mass components, $\boldsymbol{C}(\boldsymbol{\nu})$ is the matrix of the Coriolis and centripetal terms including the added mass components, $\boldsymbol{D}(\boldsymbol{\nu})$ is the damping matrix, $\boldsymbol{g}(\boldsymbol{\eta})$ is the vector of the forces and moments due to gravity, $\boldsymbol{\tau}$ is the vector of the control inputs, $\boldsymbol{g_0}$ is the vector used for ballast control, and $\boldsymbol{w}$ is the vector of forces and moments from environmental disturbances such as waves, aquatic animals, divers, etc. The details of each of these matrices is gone into in further detail in later derivations.

Before deriving this larger equation, there are some more basic equations that have to be started with. The equations for the overall forces and moments on a vehicle for translational motion and rotating motion are:

$$\boldsymbol{F} = \frac{d}{dt}(momentum) = m\left[\frac{d\boldsymbol{v}^b}{dt} + \boldsymbol{\omega}^b \times \boldsymbol{v}^b + \frac{d\boldsymbol{\omega}^b}{dt} \times \boldsymbol{R}_G + \boldsymbol{\omega}^b \times (\boldsymbol{\omega}^b \times \boldsymbol{R}_G)\right] \quad (5)$$

$$\boldsymbol{M} = \frac{d}{dt}(ang.mom.) = \boldsymbol{I} \cdot \frac{d\boldsymbol{\omega}^b}{dt} + \boldsymbol{\omega}^b \times (\boldsymbol{I} \cdot \boldsymbol{\omega}^b) + m\boldsymbol{R}_G \times \left(\frac{d\boldsymbol{v}^b}{dt} + \boldsymbol{\omega}^b \times \boldsymbol{v}^b\right) \quad (6)$$

These equations hold for a rigid body that has a fixed mass and mass distribution. The value of $\boldsymbol{I}$ is the 3x3 inertial matrix denoted as:

$$\boldsymbol{I} = \begin{bmatrix} I_x & -I_{xy} & -I_{xz} \\ -I_{xy} & I_y & -I_{yz} \\ -I_{xz} & -I_{yz} & I_z \end{bmatrix} \quad (7)$$

and the vector $\boldsymbol{R}_G$ is the location of the center of gravity in the body axes, denoted as:

$$\boldsymbol{R}_G = \begin{bmatrix} x_g \\ y_g \\ z_g \end{bmatrix} \quad (8)$$

Equations (5) and (6) can be expanded utilizing the vector components per the SNAME standard. In doing this, the first 3 equations correspond with the axial, lateral, and normal forces on the AUV due to translational motion and the last 3 equations correspond with the rolling, pitching, and yawing moments around their respective body frame axes due to rotational motion.

$$X = m\left(\dot{u} + qw - rv + x_g(-q^2 - r^2) + y_g(pq - \dot{r}) + z_g(rp + \dot{q})\right) \quad (9a)$$

$$Y = m\left(\dot{v} + ru - pw + x_g(\dot{r} + pq) + y_g(-r^2 - p^2) + z_g(-\dot{p} + rq)\right) \quad (9b)$$

$$Z = m\left(\dot{w} + pv - qu + x_g(-\dot{q} + pr) + y_g(\dot{p} + qr) + z_g(-p^2 - q^2)\right) \quad (9c)$$

$$K = I_x\dot{p} + qr\left(I_z - I_y\right) + I_{xy}(pr - \dot{q}) + I_{xz}(-\dot{r} - pq) + I_{zy}(r^2 - q^2) + m\left(y_g(\dot{w} + pv - qu) + z_g(-\dot{v} - ru + pw)\right) \quad (9d)$$

$$M = I_y\dot{q} + pr(I_x - I_z) + I_{xy}(-\dot{p} - qr) + I_{yz}(-\dot{r} + qp) + I_{xz}(-r^2 + p^2) + m\left(x_g(-\dot{w} - pv + qu) + z_g(\dot{u} + qw - rv)\right) \quad (9e)$$

$$N = I_z\dot{r} + qp\left(I_y - I_x\right) + I_{xz}(-\dot{p} + rq) + I_{yz}(-\dot{q} - rp) + I_{xy}(-p^2 + q^2) + m\left(x_g(\dot{v} + ru - pw) + y_g(-\dot{u} - qw + rv)\right) \quad (9f)$$

This set of 6 equations can be written in matrix form using the equation:

$$\boldsymbol{M_{RB}\dot{\nu} + C_{RB}\nu = \tau_{hyd}} \quad (10)$$

where $\boldsymbol{M_{RB}}$ is the rigid body inertia matrix and $\boldsymbol{C_{RB}}$ contains the Coriolis and centripetal terms. The entire 6 DOF matrices for $\boldsymbol{M_{RB}}$ and $\boldsymbol{C_{RB}}$ are:

$$\boldsymbol{M_{RB}} = \begin{bmatrix} m & 0 & 0 & 0 & mz_g & -my_g \\ 0 & m & 0 & -mz_g & 0 & mx_g \\ 0 & 0 & m & my_g & -mx_g & 0 \\ 0 & -mz_g & my_g & I_x & -I_{xy} & -I_{xz} \\ mz_g & 0 & -mx_g & -I_{yx} & I_y & -I_{yz} \\ -my_g & mx_g & 0 & -I_{xz} & -I_{yz} & I_z \end{bmatrix} \quad (11)$$

$$\boldsymbol{C_{RB}} = \begin{bmatrix} 0 & 0 & 0 \\ 0 & 0 & 0 \\ 0 & 0 & 0 \\ -m(y_gq + z_gr) & m(y_gp + w) & m(z_gp - v) \\ m(x_gq - w) & -m(z_gr + x_gp) & m(z_gq + u) \\ m(x_gr + v) & m(y_gr - u) & -m(x_gp + y_gq) \end{bmatrix}$$

$$\begin{bmatrix} m(y_gq + z_gr) & -m(x_gq - w) & -m(x_gr + v) \\ -m(y_gp + w) & m(z_gr + x_gp) & -m(y_gr - u) \\ -m(z_gp - v) & -m(z_gq + u) & m(x_gp + y_gq) \\ 0 & -I_{yz}q - I_{xz}p + I_zr & I_{yz}r + I_{xy}p - I_yq \\ I_{yz}q + I_{xz}p - I_zr & 0 & -I_{xz}r - I_{xy}q + I_xp \\ -I_{yz}r - I_{xy}p + I_yq & I_{xz}r + I_{xy}q - I_xp & 0 \end{bmatrix} \quad (12)$$

Moving to the right hand side of equation (10), $\boldsymbol{\tau_{hyd}}$ represents all of the hydrodynamic forces and moments acting on the AUV. The value of $\boldsymbol{\tau_{hyd}}$ is a sum of multiple forces which can be represented by:

$$\boldsymbol{\tau_{hyd}} = -\boldsymbol{M_A}\dot{\boldsymbol{\nu}} - \boldsymbol{C_A}\boldsymbol{\nu} - \boldsymbol{D_p}\boldsymbol{\nu} - \boldsymbol{g}(\boldsymbol{\eta}) + \boldsymbol{g_0} + \boldsymbol{\tau} + \boldsymbol{w} \tag{13}$$

where the matrices $\boldsymbol{M_A}$ and $\boldsymbol{C_A}$ represent the forces due to added mass that are proportional to vehicle accelerations, matrix $\boldsymbol{D_p}$ represents the damping forces that occur from skin friction and flow separation, the values of $\boldsymbol{g}(\boldsymbol{\eta})$ and $\boldsymbol{g_0}$ are the restoring forces attributed to gravity and buoyancy that tend to return the vehicle to equilibrium, $\boldsymbol{\tau}$ represents the control inputs, and $\boldsymbol{w}$ represents the environmental disturbances as described in equation (4). The $\boldsymbol{M_A}$, $\boldsymbol{C_A}$, $\boldsymbol{D_p}$, and $\boldsymbol{g}(\boldsymbol{\eta})$ matrices can be seen in equations (14) through (18). Each of these matrices are dependent on coefficients that are some variation of a partial derivative of a force or torque relative to a velocity or acceleration evaluated at the vehicle's origin, the details of which are covered by Orpen [16]. For this analysis, knowing the matrices is sufficient.

$$\boldsymbol{M_A} = -\begin{bmatrix} X_{\dot{u}} & X_{\dot{v}} & X_{\dot{w}} & X_{\dot{p}} & X_{\dot{q}} & X_{\dot{r}} \\ Y_{\dot{u}} & Y_{\dot{v}} & Y_{\dot{w}} & Y_{\dot{p}} & Y_{\dot{q}} & Y_{\dot{r}} \\ Z_{\dot{u}} & Z_{\dot{v}} & Z_{\dot{w}} & Z_{\dot{p}} & Z_{\dot{q}} & Z_{\dot{r}} \\ K_{\dot{u}} & K_{\dot{v}} & K_{\dot{w}} & K_{\dot{p}} & K_{\dot{q}} & K_{\dot{r}} \\ M_{\dot{u}} & M_{\dot{v}} & M_{\dot{w}} & M_{\dot{p}} & M_{\dot{q}} & M_{\dot{r}} \\ N_{\dot{u}} & N_{\dot{v}} & N_{\dot{w}} & N_{\dot{p}} & N_{\dot{q}} & N_{\dot{r}} \end{bmatrix} \tag{14}$$

$$\boldsymbol{C_A} = \begin{bmatrix} 0 & 0 & 0 & 0 & -a_3 & a_2 \\ 0 & 0 & 0 & a_3 & 0 & -a_1 \\ 0 & 0 & 0 & -a_2 & a_1 & 0 \\ 0 & -a_3 & a_2 & 0 & -b_3 & b_2 \\ a_3 & 0 & -a_1 & b_3 & 0 & -b_1 \\ -a_2 & a_1 & 0 & -b_2 & b_1 & 0 \end{bmatrix} \tag{15}$$

$$
\begin{aligned}
a_1 &= X_{\dot{u}}u + X_{\dot{v}}v + X_{\dot{w}}w + X_{\dot{p}}p + X_{\dot{q}}q + X_{\dot{r}}r \\
a_2 &= Y_{\dot{u}}u + Y_{\dot{v}}v + Y_{\dot{w}}w + Y_{\dot{p}}p + Y_{\dot{q}}q + Y_{\dot{r}}r \\
a_3 &= Z_{\dot{u}}u + Z_{\dot{v}}v + Z_{\dot{w}}w + Z_{\dot{p}}p + Z_{\dot{q}}q + Z_{\dot{r}}r \\
b_1 &= K_{\dot{u}}u + K_{\dot{v}}v + K_{\dot{w}}w + K_{\dot{p}}p + K_{\dot{q}}q + K_{\dot{r}}r \\
b_2 &= M_{\dot{u}}u + M_{\dot{v}}v + M_{\dot{w}}w + M_{\dot{p}}p + M_{\dot{q}}q + M_{\dot{r}}r \\
b_3 &= N_{\dot{u}}u + N_{\dot{v}}v + N_{\dot{w}}w + N_{\dot{p}}p + N_{\dot{q}}q + N_{\dot{r}}r
\end{aligned} \tag{16}
$$

$$
\boldsymbol{D_p} = -\begin{bmatrix}
X_u & X_v & X_w & X_p & X_q & X_r \\
Y_u & Y_v & Y_w & Y_p & Y_q & Y_r \\
Z_u & Z_v & Z_w & Z_p & Z_q & Z_r \\
K_u & K_v & K_w & K_p & K_q & K_r \\
M_u & M_v & M_w & M_p & M_q & M_r \\
N_u & N_v & N_w & N_p & N_q & N_r
\end{bmatrix} \tag{17}
$$

$$
\boldsymbol{g(\eta)} = -\begin{bmatrix}
(W-B)sin\theta \\
-(W-B)cos\theta sin\phi \\
-(W-B)cos\theta cos\phi \\
-(y_gW - y_bB)cos\theta cos\phi + (z_gW - z_bB)cos\theta sin\phi \\
(z_gW - z_bB)sin\theta + (x_gW - x_bB)cos\theta cos\phi \\
-(x_gW - x_bB)cos\theta sin\phi - (y_gW - y_bB)sin\theta
\end{bmatrix} \tag{18}
$$

where W is the weight of the vehicle and B is the buoyancy. The values of x_b, y_b, and z_b is given by $\boldsymbol{R}_B$ which is the location of the center of buoyancy in the body axis frame given by:

$$
\boldsymbol{R}_B = \begin{bmatrix} x_b \\ y_b \\ z_b \end{bmatrix} \tag{19}
$$

This completes the derivation for the rigid 6 DOF body equations as they apply to an underwater vehicle's control system.

2.4. Conclusion

This section examined the complete 6 DOF equations of motion for a rigid body. The body frame and NED frame used throughout this discussion have been defined, along with the respective terminology that accompanies motion about each of the axes.

Also covered was how to get an AUV's coordinates from the body axes in the NED frame and vice versa. After deriving the forces and moments about each of the body axes the equations were decomposed into separate matrices and the additional hydrodynamic forces were brought into consideration. The final version of the equations broken into matrix form are the most useful moving forward in the discussion.

Chapter 3

Mathematical Modeling of LoCO AUV

While knowing the rigid body 6 DOF equations of motion for underwater vehicles is a critical first step to understanding any AUV's control system, some AUV's that are limited in their design and range of motion can have a separate set of equations of motion derived from that which has already been discussed. Regardless, after the equations of motion for an AUV have been determined it is beneficial to linearize the system so basic control theory can be used in the design of the control system. Once the equations are linearized it becomes more straightforward to get a feeling for the stability of the system and to derive the final transfer functions that will be used in the control system design.

3.1. Simplified 3-Degrees of Freedom Models

As can be seen from Chapter 2's derivations for the rigid body 6 DOF underwater vehicle, the equations are highly coupled and quite complex. This model can be simplified by considering how LoCO is limited in its movement. As discussed, the rear thrusters provide forward propulsion and yaw control, allowing LoCO to move in the horizontal *xy*-plane. The center thruster provides the AUV with vertical travel and pitch control, allowing LoCO to move in the vertical *xz*-plane, about which the AUV is symmetric. Realizing this allows for the model to be simplified to 3 DOF for both the horizontal *xy*-plane and the vertical *xz*-plane, which makes the model much more manageable when designing a control system.

3.1.1. Simplified 3-Degrees of Freedom in the Horizontal Plane

Considering LoCO's movement only in the horizontal plane allows the model to be simplified to the 3 DOF of surge, sway, and yaw. All movement in the other coordinates can be disregarded. Therefore, the position and velocity vectors become:

$$\boldsymbol{\eta} = \begin{bmatrix} n \\ e \\ \psi \end{bmatrix}, \boldsymbol{\nu} = \begin{bmatrix} u \\ v \\ r \end{bmatrix} \tag{20}$$

The components in the 3 DOF matrices are the first, second, and sixth components in the full 6 DOF matrices. All of the 6x6 matrices that follow in the rigid body derivation can be reduced to 3x3 matrices by selecting the values of overlap between the first, second, and sixth rows and first, second, and sixth columns. Following the prescribed procedure for the rigid body matrices and recalling that y_g is zero, $\boldsymbol{M_{RB}}$ and $\boldsymbol{C_{RB}}$ simplify to:

$$\boldsymbol{M_{RB}} = \begin{bmatrix} m & 0 & 0 \\ 0 & m & mx_g \\ 0 & mx_g & I_z \end{bmatrix} \tag{21}$$

$$\boldsymbol{C_{RB}} = \begin{bmatrix} 0 & 0 & -m(x_g r + v) \\ 0 & 0 & mu \\ m(x_g r + v) & -mu & 0 \end{bmatrix} \tag{22}$$

The same procedure is followed to determine the matrices for the hydrodynamic forces and moments. However, simplifications can be made since LoCO is symmetrical about the *xz*-plane. Due to this symmetry, the only coefficients left are the force *X* with respect to forward velocity *u*, and the coefficients of force components *Y* and *N* with respect to velocities *v* and *r*. The linear damping matrix can be neglected as well, which provides for the $\boldsymbol{D_n}$ matrix. The hydrodynamic matrices are simplified to:

$$\boldsymbol{M_A} = -\begin{bmatrix} X_{\dot{u}} & 0 & 0 \\ 0 & Y_{\dot{v}} & Y_{\dot{r}} \\ 0 & N_{\dot{v}} & N_{\dot{r}} \end{bmatrix} \tag{23}$$

$$\boldsymbol{C_A} = \begin{bmatrix} 0 & 0 & Y_{\dot{v}}v + Y_{\dot{r}}r \\ 0 & 0 & -X_{\dot{u}}u \\ -(Y_{\dot{v}}v + Y_{\dot{r}}r) & X_{\dot{u}}u & 0 \end{bmatrix} \tag{24}$$

$$\boldsymbol{D_n} = \begin{bmatrix} X_{|u|u}|u| & 0 & 0 \\ 0 & Y_{|v|v}|v| & Y_{|r|r}|r| \\ 0 & N_{|v|v}|v| & N_{|r|r}|r| \end{bmatrix} \tag{25}$$

and $\boldsymbol{g(\eta)} = [0 \quad 0 \quad 0]^T$ since roll and pitch are both equal to zero.

That leaves for the determination of the control input $\boldsymbol{\tau}$ vector. For LoCO AUV the control input vector consists of a force for surge movement using both of the rear thrusters and a yaw moment by creating a force difference between the rear thrusters. The AUV is unable to create a sway force which sets the control input for that value to zero. The control input vector becomes:

$$\boldsymbol{\tau} = \begin{bmatrix} Forward \\ 0 \\ Torque \end{bmatrix} \qquad \begin{matrix} Forward = X_{star} + X_{port} \\ Torque = a_{rear}(X_{port} - X_{star}) \end{matrix} \tag{26}$$

where X_{star} and X_{port} are the forces from the starboard and portside rotors, respectively, and a_{rear} is the distance between the center line of the AUV to the center of the rotor.

Finally, utilizing equations (4), (10), and (13) where environmental disturbances are assumed to be negligible, the general equation for the dynamics of the vehicle can be written as:

$$(\boldsymbol{M_{RB}} + \boldsymbol{M_A})\dot{\boldsymbol{\nu}} + (\boldsymbol{C_{RB}} + \boldsymbol{C_A})\boldsymbol{\nu} + \boldsymbol{D_n}\boldsymbol{\nu} = \boldsymbol{\tau} \tag{27}$$

3.1.2. Simplified 3-Degrees of Freedom in Vertical Plane

Considering LoCO's movement only in the vertical *xz*-plane allows the model to be simplified to the 3 DOF of surge, heave, and pitch. Since the movement in all other coordinates can be disregarded, the position and velocity vectors become:

$$\boldsymbol{\eta} = \begin{bmatrix} n \\ d \\ \theta \end{bmatrix}, \ \boldsymbol{v} = \begin{bmatrix} u \\ w \\ q \end{bmatrix} \tag{28}$$

The components in the 3 DOF matrices are the first, third, and fifth components in the full 6 DOF matrices. All of the 6x6 matrices that follow in the rigid body derivation can be reduced to 3x3 matrices by selecting the values of overlap between the first, third, and fifth rows and first, third, and fifth columns. Following the prescribed procedure for the rigid body matrices and recalling that z_g is zero, $\boldsymbol{M_{RB}}$ and $\boldsymbol{C_{RB}}$ simplify to:

$$\boldsymbol{M_{RB}} = \begin{bmatrix} m & 0 & 0 \\ 0 & m & -mx_g \\ 0 & -mx_g & I_y \end{bmatrix} \tag{29}$$

$$\boldsymbol{C_{RB}} = \begin{bmatrix} 0 & 0 & -m(x_g q - w) \\ 0 & 0 & -mu \\ m(x_g q - w) & mu & 0 \end{bmatrix} \tag{30}$$

The same procedure is followed to determine the matrices for the hydrodynamic forces and moments. However, simplifications can be made since LoCO is symmetrical about the *xz*-plane. Due to this symmetry, the only coefficients left are the force *X* with respect to forward velocity *u*, and the coefficients of force components *Z* and *M* with respect to velocities *w* and *q*. The linear damping matrix can be neglected as well, which provides for the $\boldsymbol{D_n}$ matrix. The hydrodynamic matrices are simplified to:

$$\boldsymbol{M_A} = -\begin{bmatrix} X_{\dot{u}} & 0 & 0 \\ 0 & Z_{\dot{w}} & Z_{\dot{q}} \\ 0 & M_{\dot{w}} & M_{\dot{q}} \end{bmatrix} \tag{31}$$

$$\boldsymbol{C_A} = \begin{bmatrix} 0 & 0 & -(Z_{\dot{w}}w + Z_{\dot{q}}q) \\ 0 & 0 & X_{\dot{u}}u \\ Z_{\dot{w}}w + Z_{\dot{q}}q & -X_{\dot{u}}u & 0 \end{bmatrix} \tag{32}$$

$$\boldsymbol{D_n} = \begin{bmatrix} X_{|u|u}|u| & 0 & 0 \\ 0 & Z_{|w|w}|w| & Z_{|q|q}|q| \\ 0 & M_{|w|w}|w| & M_{|q|q}|q| \end{bmatrix} \tag{33}$$

and $\boldsymbol{g}(\boldsymbol{\eta}) = [0 \quad 0 \quad 0]^T$ since LoCO is designed to be neutrally buoyant and the center of gravity and center of buoyancy locations are nearly the same so that the weight minus buoyancy terms that are multiplied by the centers of gravity and buoyancy become zero.

That leaves for the determination of the control input $\boldsymbol{\tau}$ vector. For LoCO AUV the control input vector consists of a force for surge movement using both of the rear thrusters, just as in the horizontal plane, a force for heave movement using the center thruster, and a pitching moment created by use of the center thruster. The control input vector becomes:

$$\boldsymbol{\tau} = \begin{bmatrix} Forward \\ Vert \\ Pitch \end{bmatrix} \qquad \begin{matrix} Forward = X_{star} + X_{port} \\ Vert = X_{cent} \\ Pitch = X_{cent}a_{cent} \end{matrix} \tag{34}$$

where X_{cent} is the force from the central thruster and a_{cent} is the distance between the center of the center thruster and the origin of the body frame axes. Notice that the control input for the surge quantity is the same as for the horizontal plane 3 DOF simplification. As in the horizontal case, equation (27) provides the general dynamics for the 3 DOF vehicle where environmental disturbances are assumed to be negligible.

3.2. Simplified 3-Degrees of Freedom System Linearization

Although control design for non-linear systems is possible, it can be difficult to implement since non-linear systems often have control laws that are not intuitive and have very high levels of complexity which make them difficult to tune. Instead of working with a non-linear system, it is possible to linearize a system about a specific point which provides a more intuitive, tunable linear model that is not all that different from the non-linear one as long as the system operates around that point. In the case of LoCO, the idea is to linearize the system about a fixed velocity vector in the horizontal and vertical planes and only consider small deviations from that vector. Like determining the two separate 3 DOF models, the linearization has to be performed for each of the simplified models.

3.2.1. System Linearization in Horizontal Plane

Allow v_o to be the fixed velocity vector of LoCO in forward translational motion:

$$\boldsymbol{\nu}_0 = \begin{bmatrix} u_0 \\ 0 \\ 0 \end{bmatrix} \tag{35}$$

and allow $\Delta\nu$ to be the small variations about ν_o

$$\Delta\boldsymbol{\nu} = \begin{bmatrix} \Delta u \\ \Delta v \\ \Delta r \end{bmatrix} \tag{36}$$

The linearized model can be calculated from equation (27) as

$$(\boldsymbol{M_{RB}} + \boldsymbol{M_A})\Delta\dot{\boldsymbol{\nu}} + \frac{\partial \boldsymbol{f_c}}{\partial \boldsymbol{\nu}}\Big|_{\boldsymbol{\nu}_0} \Delta\nu + \frac{\partial \boldsymbol{f_d}}{\partial \boldsymbol{\nu}}\Big|_{\boldsymbol{\nu}_0} \Delta\boldsymbol{\nu} = \Delta\boldsymbol{\tau} \tag{37}$$

where

$$\boldsymbol{f_c} = (\boldsymbol{C_{RB}} + \boldsymbol{C_A})\boldsymbol{\nu} \tag{38a}$$

$$\boldsymbol{f_d = D_n \nu} \tag{38b}$$

Examining equation (37) the partial derivatives of equations (38a) and (38b) have to be taken with respect to $\boldsymbol{\nu}$. Theorem 1 as detailed and proved by Agudelo [14] allows for the partial derivatives of these to become easily calculable. The entire statement for the theorem can be read below.

Theorem 1: *Let* $\boldsymbol{x} = [x_1 \quad x_2 \quad \dots \quad x_n]^T$ *be a vector of n variables,* $\boldsymbol{H}(\boldsymbol{x})$ *a vector of q elements dependent on* $\boldsymbol{x}$*, and* $\boldsymbol{F}(\boldsymbol{x})$ *a matrix of* $p \times q$ *elements also dependent on* $\boldsymbol{x}$*. Then*

$$\frac{\partial(\boldsymbol{FH})}{\partial \boldsymbol{x}} = \boldsymbol{F}\frac{\partial \boldsymbol{H}}{\partial \boldsymbol{x}} + \frac{\partial \boldsymbol{F}}{\partial \boldsymbol{x}}(\boldsymbol{I_n} \otimes \boldsymbol{H}) \tag{39}$$

where $\boldsymbol{I_n}$ *is the identity matrix of n elements and* $\otimes$ *is the Kronecker product.*

When equation (39) from Theorem 1 is applied to equations (38a) and (38b) the following partial derivatives are discovered

$$\frac{\partial \boldsymbol{f_c}}{\partial \boldsymbol{\nu}} = \frac{\partial(\boldsymbol{C_{RB}\nu})}{\partial \boldsymbol{\nu}} + \frac{\partial(\boldsymbol{C_A\nu})}{\partial \boldsymbol{\nu}}$$

$$\frac{\partial \boldsymbol{f_c}}{\partial \boldsymbol{\nu}} = \boldsymbol{C_{RB}} + \frac{\partial \boldsymbol{C_{RB}}}{\partial \boldsymbol{\nu}}(\boldsymbol{I_3}\otimes\boldsymbol{\nu}) + \boldsymbol{C_A} + \frac{\partial \boldsymbol{C_A}}{\partial \boldsymbol{\nu}}(\boldsymbol{I_3}\otimes\boldsymbol{\nu})$$

$$\frac{\partial \boldsymbol{f_c}}{\partial \boldsymbol{\nu}} = \boldsymbol{C_{RB}} + \boldsymbol{C_A} + \left(\frac{\partial \boldsymbol{C_{RB}}}{\partial \boldsymbol{\nu}} + \frac{\partial \boldsymbol{C_A}}{\partial \boldsymbol{\nu}}\right)(\boldsymbol{I_3}\otimes\boldsymbol{\nu}) \tag{40}$$

$$\frac{\partial \boldsymbol{f_d}}{\partial \boldsymbol{\nu}} = \frac{\partial(\boldsymbol{D_n\nu})}{\partial \boldsymbol{\nu}}$$

$$\frac{\partial \boldsymbol{f_d}}{\partial \boldsymbol{\nu}} = \boldsymbol{D_n} + \frac{\partial \boldsymbol{D_n}}{\partial \boldsymbol{\nu}}(\boldsymbol{I_3}\otimes\boldsymbol{\nu}) \tag{41}$$

where

$$\frac{\partial \boldsymbol{C_{RB}}}{\partial \boldsymbol{\nu}} = \begin{bmatrix} 0 & 0 & 0 & 0 & 0 & -m & 0 & 0 & -mx_g \\ 0 & 0 & m & 0 & 0 & 0 & 0 & 0 & 0 \\ 0 & -m & 0 & m & 0 & 0 & mx_g & 0 & 0 \end{bmatrix} \tag{42}$$

$$\frac{\partial \boldsymbol{C_A}}{\partial \boldsymbol{\nu}} = \begin{bmatrix} 0 & 0 & 0 & 0 & 0 & Y_{\dot{v}} & 0 & 0 & Y_{\dot{r}} \\ 0 & 0 & -X_{\dot{u}} & 0 & 0 & 0 & 0 & 0 & 0 \\ 0 & X_{\dot{u}} & 0 & -Y_{\dot{v}} & 0 & 0 & -Y_{\dot{r}} & 0 & 0 \end{bmatrix} \tag{43}$$

$$\frac{\partial \boldsymbol{D_n}}{\partial \boldsymbol{\nu}} = -\begin{bmatrix} X_{|u|u}sgn(u) & 0 & 0 & 0 & 0 & 0 & 0 & 0 & 0 \\ 0 & 0 & 0 & 0 & Y_{|v|v}sgn(v) & 0 & 0 & 0 & Y_{|r|r}sgn(r) \\ 0 & 0 & 0 & 0 & N_{|v|v}sgn(v) & 0 & 0 & 0 & N_{|r|r}sgn(r) \end{bmatrix} \tag{44}$$

The Laplace transform can be applied to the linearized model given by equation (37) so that the linearized model takes the form:

$$\left((\boldsymbol{M_{RB}} + \boldsymbol{M_A})s + \boldsymbol{C_{RB}} + \boldsymbol{C_A} + \boldsymbol{D_n} + \left(\frac{\partial \boldsymbol{C_{RB}}}{\partial \boldsymbol{\nu}} + \frac{\partial \boldsymbol{C_A}}{\partial \boldsymbol{\nu}} + \frac{\partial \boldsymbol{D_n}}{\partial \boldsymbol{\nu}}\right)(\boldsymbol{I_3} \otimes \boldsymbol{\nu})\right)\Big|_{\boldsymbol{\nu}_0} \boldsymbol{\nu}(s) = \boldsymbol{\tau}(s) \tag{45}$$

Equation (45) can be solved for using all of the matrices derived in section (3.1.1) along with the partial derivative matrices solved for in equations (42) through (44). This gives

$$\begin{bmatrix} m_u s - 2|u|X_{|u|u} & -m_v r & -m_v v - 2m_{Y_{\dot{r}}} r \\ m_u r & m_v s - 2|v|Y_{|v|v} & m_{Y_{\dot{r}}} s + m_u u - 2|r|Y_{|r|r} \\ -m_{uv} v + m_{Y_{\dot{r}}} r & m_{N_{\dot{v}}} s - m_{uv} u - 2|v|N_{|v|v} & m_r s + m_{Y_{\dot{r}}} u - 2|r|N_{|r|r} \end{bmatrix}_{\boldsymbol{\nu}_0} \boldsymbol{\nu}(s) = \boldsymbol{\tau}(s)$$

$$\begin{bmatrix} m_u s - 2|u_o|X_{|u|u} & 0 & 0 \\ 0 & m_v s & m_{Y_{\dot{r}}} s + m_u u_o \\ 0 & m_{N_{\dot{v}}} s - m_{uv} u_o & m_r s + m_{Y_{\dot{r}}} u_o \end{bmatrix} \boldsymbol{\nu}(s) = \boldsymbol{\tau}(s) \tag{46}$$

where

$$m_u = m - X_{\dot{u}} \tag{47a}$$

$$m_v = m - Y_{\dot{v}} \tag{47b}$$

$$m_{uv} = m_u - m_v = Y_{\dot{v}} - X_{\dot{u}} \tag{47c}$$

$$m_{Y_{\dot{r}}} = mx_g - Y_{\dot{r}} \tag{47d}$$

$$m_{N_{\dot{v}}} = mx_g - N_{\dot{v}} \tag{47e}$$

$$m_r = I_z - N_{\dot{r}} \tag{47f}$$

Equation (46) is the final solved matrix of the Laplace transform of the linearized model in the horizontal plane.

3.2.2. System Linearization in Vertical Plane

The equation (35) for vector $\boldsymbol{\nu}_0$ will again be used for the fixed velocity vector, but $\Delta\boldsymbol{\nu}$ becomes:

$$\Delta\boldsymbol{\nu} = \begin{bmatrix} \Delta u \\ \Delta w \\ \Delta q \end{bmatrix} \tag{48}$$

The linearized model and the partial derivative equations remain the same for the motion in the vertical plane. The partial derivates must be changed based on the vertical *xz*-plane specific matrices derived in section (3.1.2). The partial derivative matrices become:

$$\frac{\partial \boldsymbol{C_{RB}}}{\partial \boldsymbol{\nu}} = \begin{bmatrix} 0 & 0 & 0 & 0 & 0 & m & 0 & 0 & -mx_g \\ 0 & 0 & -m & 0 & 0 & 0 & 0 & 0 & 0 \\ 0 & m & 0 & -m & 0 & 0 & mx_g & 0 & 0 \end{bmatrix} \tag{49}$$

$$\frac{\partial \boldsymbol{C_A}}{\partial \boldsymbol{\nu}} = \begin{bmatrix} 0 & 0 & 0 & 0 & 0 & -Z_{\dot{w}} & 0 & 0 & -Z_{\dot{q}} \\ 0 & 0 & X_{\dot{u}} & 0 & 0 & 0 & 0 & 0 & 0 \\ 0 & -X_{\dot{u}} & 0 & Z_{\dot{w}} & 0 & 0 & Z_{\dot{q}} & 0 & 0 \end{bmatrix} \tag{50}$$

$$\frac{\partial \boldsymbol{D_n}}{\partial \boldsymbol{\nu}} = -\begin{bmatrix} X_{|u|u}sgn(u) & 0 & 0 & 0 & 0 & 0 & 0 & 0 & 0 \\ 0 & 0 & 0 & 0 & Z_{|w|w}sgn(w) & 0 & 0 & 0 & Z_{|q|q}sgn(q) \\ 0 & 0 & 0 & 0 & M_{|w|w}sgn(w) & 0 & 0 & 0 & M_{|q|q}sgn(q) \end{bmatrix} \tag{51}$$

Equation (37) can be solved for using the matrices derived in section (3.1.2) along with the partial derivative matrices solved for in equations (49) through (51). This gives

$$\begin{bmatrix} m_u s - 2|u|X_{|u|u} & m_w q & m_w w - 2m_{Z_{\dot{q}}} q \\ -m_u q & m_w s - 2|w|Z_{|w|w} & -m_{Z_{\dot{q}}} s - m_u u - 2|q|Z_{|q|q} \\ m_{uw} w + m_{Y_{\dot{q}}} q & -m_{M_{\dot{w}}} s + m_{uw} u - 2|w|M_{|w|w} & m_q s + m_{Z_{\dot{q}}} u - 2|q|M_{|q|q} \end{bmatrix}_{\boldsymbol{\nu}_0} \boldsymbol{\nu}(s) = \boldsymbol{\tau}(s)$$

$$\begin{bmatrix} m_u s - 2|u_0|X_{|u|u} & 0 & 0 \\ 0 & m_w s & -m_{Z_{\dot{q}}} s - m_u u_0 \\ 0 & -m_{M_{\dot{w}}} s + m_{uw} u_0 & m_q s + m_{Z_{\dot{q}}} u_0 \end{bmatrix} \boldsymbol{\nu}(s) = \boldsymbol{\tau}(s) \qquad (52)$$

where

$$m_u = m - X_{\dot{u}} \qquad (53a)$$

$$m_w = m - Z_{\dot{w}} \qquad (53b)$$

$$m_{uw} = m_u - m_w = Z_{\dot{w}} - X_{\dot{u}} \qquad (53c)$$

$$m_{Z_{\dot{q}}} = m x_g + Z_{\dot{q}} \qquad (53d)$$

$$m_{M_{\dot{w}}} = m x_g + M_{\dot{w}} \qquad (53e)$$

$$m_q = I_y - M_{\dot{q}} \qquad (53f)$$

Equation (52) is the final solved matrix of the Laplace transform of the linearized model for the motion in the vertical *xz*-plane.

3.3. Stability of Simplified, Linearized Systems

Dynamic stability is the tendency of a system to return to its original state after being disturbed from equilibrium. While it can be advantageous to design a system to have unstable characteristics, the LoCO control system is being designed with stability in mind given its focus on video imaging and the incredibly dynamic environment it is set to work in. Stability is determined by calculating the poles of a linearized model. If each of the poles has negative real part the system is a stable one. On the other hand, if at least one pole has positive real part the system is unstable. Having already calculated the

linearized models for the horizontal and vertical planes that LoCO can control in, stability can begin to be analyzed.

3.3.1. Stability Analysis of the Horizontal Plane System

The poles of the horizontal plane system can be determined by taking the determinant of the matrix in equation (46) and setting it equal to zero.

$$\begin{vmatrix} m_u s - 2|u_0|X_{|u|u} & 0 & 0 \\ 0 & m_v s & m_{Y_{\dot{r}}} s + m_u u_0 \\ 0 & m_{N_{\dot{v}}} s - m_{uv} u_0 & m_r s + m_{Y_{\dot{r}}} u_0 \end{vmatrix} = 0$$

$$\left(m_u s - 2|u_0|X_{|u|u}\right)\left(m_v s\left(m_r s + m_{Y_{\dot{r}}} u_0\right) - \left(m_{N_{\dot{v}}} s - m_{uv} u_0\right)\left(m_{Y_{\dot{r}}} s + m_u u_0\right)\right) = 0 \quad (54)$$

Examining equation (54) the first pole is given by

$$m_u s - 2|u_0|X_{|u|u} = 0$$

$$s = 2|u_0|\frac{X_{|u|u}}{m_u} \quad (55)$$

To ensure that it has real negative part the inequality

$$\frac{X_{|u|u}}{m_u} = \frac{X_{|u|u}}{m - X_{\dot{u}}} < 0 \quad (56)$$

has to hold. This is always achieved since dynamic drag implies that the coefficients of $X_{|u|u}$ and $X_{\dot{u}}$ are negative. This provides a negative value in the numerator and a positive value in the denominator since mass is always a positive real number, which means the inequality holds.

The calculation of the other two poles is more complex since the remaining part of the left hand side of equation (54) has to be factored. Nonetheless, the calculation is shown to be:

$$m_v s\left(m_r s + m_{Y_{\dot{r}}} u_0\right) - \left(m_{N_{\dot{v}}} s - m_{uv} u_0\right)\left(m_{Y_{\dot{r}}} s + m_u u_0\right) = 0$$

$$s^2\left(m_v m_r - m_{Y_{\dot{r}}} m_{N_{\dot{v}}}\right) + s u_0\left(m_{Y_{\dot{r}}}(m_{uv} + m_v) - m_{N_{\dot{v}}} m_u\right) + m_u m_{uv} u_0^2 = 0$$

$$s^2\left(m_v m_r - m_{Y_{\dot{r}}} m_{N_{\dot{v}}}\right) + s u_0\left(m_{Y_{\dot{r}}} m_u - m_{N_{\dot{v}}} m_u\right) + m_u m_{uv} u_0^2 = 0$$

$$s^2\left(m_v m_r - m_{Y_{\dot{r}}} m_{N_{\dot{v}}}\right) + s u_0 m_u\left(m_{Y_{\dot{r}}} - m_{N_{\dot{v}}}\right) + m_u m_{uv} u_0^2 = 0$$

$$s^2\left(m_v m_r - m_{Y_{\dot{r}}} m_{N_{\dot{v}}}\right) + s u_0 m_u (N_{\dot{v}} - Y_{\dot{r}}) + m_u m_{uv} u_0^2 = 0$$

$$s^2 + s\frac{u_0 m_u (N_{\dot{v}} - Y_{\dot{r}})}{\left(m_v m_r - m_{Y_{\dot{r}}} m_{N_{\dot{v}}}\right)} + \frac{m_u m_{uv} u_0^2}{\left(m_v m_r - m_{Y_{\dot{r}}} m_{N_{\dot{v}}}\right)} = 0 \tag{57}$$

If one takes the second term in equation (57) to be B, and takes the third term to be C, the quadratic equation can be used to find the remaining two poles.

$$s_{1,2} = -\frac{B}{2} \pm \frac{\sqrt{B^2 - 4C}}{2} \tag{58}$$

If $\sqrt{B^2 - 4C} < 0$ the poles are complex and the real part becomes determined by $-\frac{B}{2}$. Therefore, as long as the value of B is positive, the system is stable. In this case C is also positive since $B^2 < 4C$.

If $\sqrt{B^2 - 4C} > 0$ the poles are entirely real. In order to be negative, the values of B and C are determined to be:

$$-\frac{B}{2} \pm \frac{\sqrt{B^2 - 4C}}{2} \leq 0$$

$$B \geq \pm\sqrt{B^2 - 4C}$$

$$B \geq 0 \tag{59a}$$

$$B \geq \pm\sqrt{B^2 - 4C}$$

$$B^2 \geq B^2 - 4C$$

$$C \geq 0 \tag{59b}$$

In order for the system to be stable in the case that the poles are not complex, both B and C have to be greater than or equal to zero. From this analysis it is realized that stability is directly tied to the signs of B and C, which are directly tied to the drag coefficient values of LoCO.

3.3.2. Stability Analysis of the Vertical Plane System

The poles of the vertical xz-plane system can be determined by taking the determinant of the matrix in equation (52) and setting it equal to zero.

$$\begin{vmatrix} m_u s - 2|u_0|X_{|u|u} & 0 & 0 \\ 0 & m_w s & -m_{Z_{\dot{q}}} s - m_u u_0 \\ 0 & -m_{M_{\dot{w}}} s + m_{uw} u_0 & m_q s + m_{Z_{\dot{q}}} u_0 \end{vmatrix} = 0$$

$$\left(m_u s - 2|u_0|X_{|u|u}\right)\left(m_w s\left(m_q s + m_{Z_{\dot{q}}} u_0\right) - \left(-m_{M_{\dot{w}}} s + m_{uw} u_0\right)\left(-m_{Z_{\dot{q}}} s - m_u u_0\right)\right) = 0 \quad (60)$$

The first pole for the vertical plane analysis matches the first pole for the horizontal plane analysis and is always negative due to the existence of dynamic drag implying that $X_{|u|u}$ and $X_{\dot{u}}$ are negative.

The calculation of the other two poles is more complex since the remaining part of the left hand side of equation (60) has to be factored. Nonetheless, the calculation is shown to be:

$$m_w s\left(m_q s + m_{Z_{\dot{q}}} u_0\right) - \left(-m_{M_{\dot{w}}} s + m_{uw} u_0\right)\left(-m_{Z_{\dot{q}}} s - m_u u_0\right) = 0$$

$$s^2\left(m_w m_q - m_{M_{\dot{w}}} m_{Z_{\dot{q}}}\right) + s u_0\left(m_{Z_{\dot{q}}}(m_w + m_{uw}) - m_{M_{\dot{w}}} m_u\right) + m_u m_{uw} u_0^2 = 0$$

$$s^2\left(m_w m_q - m_{M_{\dot{w}}} m_{Z_{\dot{q}}}\right) + s u_0\left(m_{Z_{\dot{q}}} m_u - m_{M_{\dot{w}}} m_u\right) + m_u m_{uw} u_0^2 = 0$$

$$s^2\left(m_w m_q - m_{M_{\dot{w}}} m_{Z_{\dot{q}}}\right) + s u_0 m_u\left(m_{Z_{\dot{q}}} - m_{M_{\dot{w}}}\right) + m_u m_{uw} u_0^2 = 0$$

$$s^2\left(m_w m_q - m_{M_{\dot{w}}} m_{Z_{\dot{q}}}\right) + s u_0 m_u\left(Z_{\dot{q}} - M_{\dot{w}}\right) + m_u m_{uw} u_0^2 = 0$$

$$s^2 + s\frac{u_0 m_u (Z_{\dot{q}} - M_{\dot{w}})}{\left(m_w m_q - m_{M_{\dot{w}}} m_{Z_{\dot{q}}}\right)} + \frac{m_u m_{uw} u_0^2}{\left(m_w m_q - m_{M_{\dot{w}}} m_{Z_{\dot{q}}}\right)} = 0 \quad (61)$$

If one takes the second term in equation (61) to be B, and takes the third term to be C, the quadratic equation can be used to find the remaining two poles.

$$s_{1,2} = -\frac{B}{2} \pm \frac{\sqrt{B^2 - 4C}}{2} \quad (62)$$

The analysis remains the same as for the horizontal plane where the value of B has to be positive if the pole is a complex conjugate, or the values of B and C both have to be greater than or equal to zero if the poles only have real part. Regardless, stability is still tied directly to the signs of B and C which are directly tied to the drag coefficient values of LoCO.

3.4. Transfer Functions of Simplified, Linearized 3-Degrees of Freedom Systems

The purpose of transfer functions are to directly relate a system's outputs to its inputs. After simplifying and linearizing each of the 3 DOF systems, along with investigating the stability of each of the systems, determining the transfer functions of each of the systems becomes straightforward.

3.4.1. Transfer Functions of Horizontal Plane System

The transfer function relates the velocity vector $\boldsymbol{\nu}(s)$ of the horizontal plane system to the controller inputs $\boldsymbol{\tau}(s)$ in the complex domain. From equation (46):

$$\frac{\boldsymbol{\nu}(s)}{\boldsymbol{\tau}(s)} = \begin{bmatrix} m_u s - 2|u_0|X_{|u|u} & 0 & 0 \\ 0 & m_v s & m_{Y_{\dot{r}}} s + m_u u_0 \\ 0 & m_{N_{\dot{v}}} s - m_{uv} u_0 & m_r s + m_{Y_{\dot{r}}} u_0 \end{bmatrix}^{-1}$$

$$\frac{\boldsymbol{\nu}(s)}{\boldsymbol{\tau}(s)} = \begin{bmatrix} \frac{1}{m_u s - 2|u_0|X_{|u|u}} & 0 & 0 \\ 0 & \begin{bmatrix} m_r s + m_{Y_{\dot{r}}} u_0 & -m_{Y_{\dot{r}}} s - m_u u_0 \\ -m_{N_{\dot{v}}} s + m_{uv} u_0 & m_v s \end{bmatrix} & \\ 0 & \frac{}{s^2\left(m_v m_r - m_{Y_{\dot{r}}} m_{N_{\dot{v}}}\right) + s u_0 m_u (N_{\dot{v}} - Y_{\dot{r}}) + m_u m_{uv} u_0^2} & \end{bmatrix} \tag{63}$$

The transfer functions of interest are those on the diagonal that are not equal to zero since they correlate with the forward velocity with respect to the propulsive forces from the rotors, and the angular velocity with respect to the moment created by the difference in force between the two rotors. With that in mind, the transfer functions of interest are:

$$\frac{u(s)}{Forward(s)} = \frac{1}{m_u s - 2|u_0|X_{|u|u}} \tag{64}$$

$$\frac{r(s)}{Torque(s)} = \frac{m_v s}{s^2\left(m_v m_r - m_{Y_{\dot{r}}} m_{N_{\dot{v}}}\right) + s u_0 m_u (N_{\dot{v}} - Y_{\dot{r}}) + m_u m_{uv} u_0^2} \tag{65}$$

These transfer functions are the basis for the study of LoCO's behavior near specific forward velocities.

3.4.2. Transfer Function of Vertical Plane System

The transfer function relates the velocity vector $\boldsymbol{\nu}(s)$ of the vertical xz-plane system to the controller inputs $\boldsymbol{\tau}(s)$ in the complex domain. From equation (52):

$$\frac{\boldsymbol{\nu}(s)}{\boldsymbol{\tau}(s)} = \begin{bmatrix} m_u s - 2|u_0|X_{|u|u} & 0 & 0 \\ 0 & m_w s & -m_{Z_{\dot{q}}} s - m_u u_0 \\ 0 & -m_{M_{\dot{w}}} s + m_{uw} u_0 & m_q s + m_{Z_{\dot{q}}} u_0 \end{bmatrix}^{-1}$$

$$\frac{\nu(s)}{\tau(s)} = \begin{bmatrix} \frac{1}{m_u s - 2|u_0|X_{|u|u}} & 0 & 0 \\ 0 & \begin{bmatrix} m_q s + m_{Z_{\dot{q}}} u_0 & m_{Z_{\dot{q}}} s + m_u u_0 \\ m_{M_{\dot{w}}} s - m_{uw} u_0 & m_w s \end{bmatrix} & \\ 0 & \frac{}{s^2\left(m_w m_q - m_{M_{\dot{w}}} m_{Z_{\dot{q}}}\right) + s u_0 m_u (Z_{\dot{q}} - M_{\dot{w}}) + m_u m_{uw} u_0^2} & \end{bmatrix} \tag{66}$$

The transfer functions of interest are those on the diagonal since they correlate with the forward velocity with respect to the propulsive forces from the rotors, the heave

velocity with respect to the propulsive force from the central rotor, and the angular velocity with respect to the moment created by the central rotor that drives pitching motion. With that in mind, the transfer functions of interest are:

$$\frac{u(s)}{Forward(s)} = \frac{1}{m_u s - 2|u_0|X_{|u|u}} \tag{67}$$

$$\frac{w(s)}{Vert(s)} = \frac{m_q s + m_{Z_{\dot{q}}} u_0}{s^2\left(m_w m_q - m_{M_{\dot{w}}} m_{Z_{\dot{q}}}\right) + s u_0 m_u (Z_{\dot{q}} - M_{\dot{w}}) + m_u m_{uw} u_0^2} \tag{68}$$

$$\frac{q(s)}{Pitch(s)} = \frac{m_w s}{s^2\left(m_w m_q - m_{M_{\dot{w}}} m_{Z_{\dot{q}}}\right) + s u_0 m_u (Z_{\dot{q}} - M_{\dot{w}}) + m_u m_{uw} u_0^2} \tag{69}$$

These transfer functions are the basis for the study of LoCO's behavior near specific forward velocities in the vertical *xz*-plane.

Chapter 4

LoCO Autopilot

Now that the transfer functions that define LoCO's motion have been determined the control system can undergo its design phase. Before jumping into the design of the system there are a number of control performance characteristics defined along with their relevancy to LoCO's motion. Additionally, a brief overview of PID controllers is provided in the interest of those who will be using LoCO and may want to modify the control characteristics.

4.1. Control Characteristics

There are a number of important control terms that characterize the controller performance. The four most relative to and directly manageable by PID controllers are steady state error, settling time, rise time, and maximum overshoot. Changing the values of these four characteristics will determine the level of tuning required from the LoCO controller which will ultimately decide how LoCO performs.

To start, steady state error is the measure of the real output of a system compared to the desired output of the system as time goes to infinity. Ideally, this value would be zero and the system would be able to operate with no amount of error indefinitely. Realistically, systems are always going to have some amount of error inherent to them. The goal of most systems is to minimize this error and get it within an acceptable range. The acceptable range for different systems varies, but typically a range between 2 and 5% of the desired steady state value is sufficient.

Directly tied to steady state is settling time. Settling time is defined as the amount of time required for a system to reach its steady state error condition. Typically, a system is considered to have reached its steady state condition once it remains within a band of approximately ±2-5% of the specified value. It is desirable for settling time to be relatively low since that will have meant that the steady state condition has been reached sooner. A low settling time also correlates with less oscillations about the steady state value. Settling time for LoCO will vary with the velocity it is being asked to maintain.

Next up is rise time which is defined as the time it takes for the system to go from 10% of steady state condition to 90% of steady state condition. It is defined this way since the first and final 10% of reaching steady state tends to take a bit longer. In this way the primarily linear part of the motion is captured. Rise time can be thought of as how quickly changes to the system can be made. In LoCO's case, the rise time is going to be selected so that a discrete amount of change consistently happens over a similar period of time regardless of the current condition.

Finally, maximum overshoot is defined as the maximum amount the response of a system goes above the steady state value and is defined as a percentage of that steady state value. In most cases it is desirable to minimize the maximum overshoot without entirely undershooting the system. Cases where a large maximum overshoot is common is when the system is being asked for too quick of a response time, responds accordingly, but is then unable to slow itself down enough before it reaches steady state conditions. Additionally, a system with a high maximum overshoot value is more likely to have a larger number of continued oscillations before reaching steady state. For LoCO this will have to be balanced with the rise time of the system.

4.2. PID Control

The term PID stands for proportional-integral-derivative control. Controllers do not have to have all three components to their control system. Some controllers use some combination and, in some cases, it is sufficient to use only one. PID controllers are relatively popular since they are some of the easiest to implement and understand at a fundamental level. They also tend to be a good starting controller when beginning to work on a system since they can be augmented by more robust, technically difficult methods of control as more is learned about the system and its requirements.

Proportional control multiplies the error by a set gain value to amplify the amount of error the system is experiencing. Because it is directly multiplied with the error, it provides a small amount of control when the system has a small error or is close to steady state and provides a larger amount of control when the system has a large error. This type of controller experiences exponential convergence and is unable to completely get rid of steady-state error on its own.

The integral control is an integrating term that provides the system with feedback based on past values of the error signal. With this, an integral controller tends to be best at eliminating steady-state error. The drawback to this type of controller is that it tends to increase a system's level of maximum overshoot. It also takes a bit for this part of the system to respond since it has to look at past data and trends within the system before it is able to respond. Therefore, if a system is changing rapidly and often an integral controller may not optimal but may still be used with other methods of control to reduce steady state error.

Finally, the derivative controller provides feedback based on predicted future values of a system's error signal. This is beneficial in that it tends to have a faster response time than proportional and integral controllers, but since it is anticipatory it can increase error if it predicts the error trend incorrectly. Additionally, if a system has a huge amount of error but that error is not changing, the derivative controller will provide no level of control since it relies on the future trend to control. That said, a derivative controller is fairly good at reducing oscillations in a system since it is predictive.

4.3. LoCO Control

The transfer functions that are going to allow for control can be seen in equations (64), (65), (68), and (69). Equation (67) was omitted since it is the same as equation (64). In order to solve these equations, the hydrodynamic forces and moments acting on LoCO during operation have to be determined. Orpen [16] determines these values in his work which are in Table 1 on the next page. These values are used to put the transfer functions in a numerical form.

It is important to recall that the transfer functions were created by linearizing the 3 DOF equations of motion about a specific velocity which was left as a variable for purposes of derivation. In order to bring the transfer functions into a numerical form a specific velocity now has to be selected. LoCO has a maximum speed of 1.5 meters per second, but often does not operate at that speed. For LoCO's case it is going to be best to create variations of the control system for different velocities to give LoCO the best shot at operating as anticipated. The four velocities at which LoCO's transfer functions are solved are 0.3 meter per second, 0.7 meters per second, 1.1 meters per second, and 1.5 meters per second.

Parameter Description	Variable	Value	Units
Mass	m	12.5450	kg
Moments of Inertia	I_{xx}	0.1909	kg/m^2
	I_{yy}	1.2050	kg/m^2
	I_{zz}	1.3465	kg/m^2
	I_{xy}	0.002257	kg/m^2
	I_{yz}	-0.0002695	kg/m^2
	I_{xz}	0.005911	kg/m^2
Center of Gravity	x_g	0.2538	m
	y_g	0.001019	m
	z_g	0.002130	m
Center of Buoyancy	x_b	0.2417	m
	y_b	-4.84E-09	m
	z_b	5.17E-05	m
Added Mass Coefficients	$X_{\dot{u}}$	2.8992	kg
	$Y_{\dot{v}}$	11.8555	kg
	$Z_{\dot{w}}$	12.9146	kg
	$K_{\dot{p}}$	0.1356	kg·m^2
	$M_{\dot{q}}$	1.4260	kg·m^2
	$N_{\dot{r}}$	1.0667	kg·m^2
	$Z_{\dot{q}}$	-3.5616	kg·m
	$M_{\dot{w}}$	-3.5616	kg·m
	$Y_{\dot{r}}$	2.8183	kg·m
	$N_{\dot{v}}$	2.8183	kg·m
Hydrodynamic Damping Coefficients	$X_{\|u\|u}$	-23.1450	kg/m
	$Y_{\|v\|v}$	-84.5565	kg/m
	$Z_{\|w\|w}$	-100.9333	kg/m
	$K_{\|p\|p}$	-0.09952	kg·m^2
	$M_{\|q\|q}$	-3.2367	kg·m^2
	$N_{\|r\|r}$	-2.8312	kg·m^2
	$M_{\|w\|w}$	20.5522	kg
	$N_{\|v\|v}$	-18.6032	kg

Table 1: *LoCO Design and Hydrodynamic Characteristics*

The solved transfer functions around each of the selected velocities can be seen in Table 2.

Transfer Function	Velocity (m/s)	Numerical Transfer Function
$\frac{u(s)}{Prop}$	0.3	$\frac{1}{9.6458s + 13.8870}$
	0.7	$\frac{1}{9.6458s + 32.4030}$
	1.1	$\frac{1}{9.6458s + 50.9190}$
	1.5	$\frac{1}{9.6458s + 69.4350}$
$\frac{r(s)}{Torque}$	0.3	$\frac{0.6895s}{0.0592s^2 + 7.7752}$
	0.7	$\frac{0.6895s}{0.0592s^2 + 42.3314}$
	1.1	$\frac{0.6895s}{0.0592s^2 + 104.5327}$
	1.5	$\frac{0.6895s}{0.0592s^2 + 194.3790}$
$\frac{w(s)}{Vert}$	0.3	$\frac{-0.2210s - 0.1133}{-0.0610s^2 + 8.6946}$
	0.7	$\frac{-0.2210s - 0.2644}{-0.0610s^2 + 47.3372}$
	1.1	$\frac{-0.2210s - 0.4154}{-0.0610s^2 + 116.8939}$
	1.5	$\frac{-0.2210s - 0.5665}{-0.0610s^2 + 217.3647}$
$\frac{q(s)}{Pitch}$	0.3	$\frac{-0.3696s}{-0.0610s^2 + 8.6946}$
	0.7	$\frac{-0.3696s}{-0.0610s^2 + 47.3372}$
	1.1	$\frac{-0.3696s}{-0.0610s^2 + 116.8939}$
	1.5	$\frac{-0.3696s}{-0.0610s^2 + 217.3647}$

Table 2: *Transfer Function Equations about Specific Velocity*

For the LoCO system it is desirable to have low steady state error. This lends itself well to investigating a PI controller for use in the system. Additionally, it is beneficial for LoCO to have a controller that is able to stabilize LoCO at steady state with minimal oscillations. This suggests the use of a PID controller. Depending on the type of motion one controller may work better than the other. Because of this, a PI and PID controller was determined for each set of equations for a linearizing velocity.

4.3.1. PI Controllers

For each of the four linearizing velocities a series of four PI controllers is created. Each of these four PI controllers exerts control over one of the four motions that LoCO is capable of controlling in. The values of the proportional and integral gains are determined using MATLAB's 'pidTuner' function. This function analyzes the input transfer function as a simple step function and optimizes it for user chosen response time relative to the system's capability and transient behavior. For the purposes of this control system a middle of the road response time was selected for each of the controllers, neither erring on the side of fast or slow response time. For transient behavior, the system was designed to be more robust than it was aggressive since LoCO's use cases lend themselves to slower, but deliberate work over quick and haphazard. MATLAB was also used to quantify the characterizing system parameters of rise time, settling time, and maximum overshoot as a percentage of the final steady state value. For each velocity that each of the four motions was linearized for, the values of the gains and characterizing system parameters can be seen in Table 3.

Velocity	Motion	K_P	K_I	Rise Time (s)	Settling Time (s)	Maximum Overshoot
0.3 m/s	Surge	14.4759	62.6465	0.562	2.06	13.8%
	Yaw	9.7265	740.171	0.00939	0.0730	25.2%
	Heave	24.9323	1460.13	0.0120	0.632	26.4%
	Pitch	422.690	623,533	0.00429	0.00343	26.2%
0.7 m/s	Surge	33.7770	340.531	0.241	0.881	13.8%
	Yaw	22.6951	4029.80	0.00403	0.0313	25.2%
	Heave	58.1796	7950.75	0.00516	0.270	26.4%
	Pitch	2301.33	18,482,300	7.87e-05	6.29e-04	26.2%
1.1 m/s	Surge	53.0782	840.902	0.153	0.561	13.8%
	Yaw	35.6638	9951.13	0.00256	0.0199	25.2%
	Heave	91.4141	19,628.8	0.00328	0.172	26.4%
	Pitch	5682.88	112,705,000	3.19e-05	2.55e-05	26.2%
1.5 m/s	Surge	72.3794	1563.66	0.112	0.411	13.8%
	Yaw	48.6325	18,504.2	0.00188	0.0146	25.2%
	Heave	124.661	36,503.2	0.00241	0.126	26.4%
	Pitch	10,567.3	389,707,000	1.71e-05	1.37e-04	26.2%

Table 3: *LoCO PI Controller Gains and Characteristics*

As can be seen from the table, the values for the gains of the controllers generally increases as the velocity increases. With this, the rise times and settling times for one kind of motion generally decreases. This is as expected since faster velocities will require more power from the thrusters and a faster acceleration, which also means that they will reach and begin to oscillate about the desired steady state value more quickly. Likewise, being able to control so finely and quickly requires for higher gains from the controller.

Each of the controllers detailed in Table 3 is a stable controller that uses feedback to reach the desired steady state value. This is critical considering the motions of heave and pitch in the vertical *xz*-plane have been calculated to be inherently unstable for LoCO. The gains for these motions, especially that of pitch, seem unreasonably high, and they are tied directly to the incredibly low rise and settling times for this type of motion. While the controller will supposedly be able to successfully control for the designed

system, it is believed that there may be some miscalculations for this portion of the control system. These miscalculations are believed to come from sources of error within the hydrodynamic and added mass equations. While the controller may be able to successfully control within a simulation that uses these erroneous hydrodynamic and added mass equations, it may not fare so well in the real world.

4.3.2. PID Controllers

Similar to the PI controller, for each of the four linearizing velocities a series of four PID controllers is created. Again, each of these four PID controllers exerts control over one of the four motions that LoCO is capable of controlling in. MATLAB's 'pidTuner' function was utilized to determine the proportional, integral, and derivative gains with the same user inputs as for the PI controller. MATLAB was again used to quantify the characterizing system parameters of rise time, settling time, and maximum overshoot as a percentage of the final steady state value. For each velocity that each of the four motions was linearized for, the values of the gains and characterizing system parameters can be seen in Table 4.

Velocity	Motion	K_P	K_I	K_D	Rise Time (s)	Settling Time (s)	Maximum Overshoot
0.3 m/s	Surge	19.8801	51.8782	0.0	0.634	2.20	6.08%
	Yaw	17.5461	720.500	0.0	0.00729	0.0608	12.7%
	Heave	23.0649	1639.22	0.081135	0.0139	0.895	26.7%
	Pitch	168.351	17,000.2	0.022269	0.00153	0.0235	19.3%
0.7 m/s	Surge	46.3870	282.448	0.0	0.272	0.942	6.08%
	Yaw	40.9408	3922.70	0.0	0.00313	0.0260	12.7%
	Heave	53.8220	8925.92	0.081135	0.00594	0.383	26.7%
	Pitch	916.575	503,918	0.022269	2.81e-04	0.00431	19.3%
1.1 m/s	Surge	72.8938	697.473	0.0	0.173	0.600	6.08%
	Yaw	64.3356	9686.67	0.0	0.00199	0.0166	12.7%
	Heave	84.5675	22,036.3	0.081135	0.00378	0.244	26.7%
	Pitch	2263.38	3,072,830	0.022269	1.14e-04	0.00175	19.3%

1.5 m/s	Surge	99.4006	1296.95	0.0	0.127	0.440	6.08%
	Yaw	87.7304	18,012.4	0.0	0.00146	0.0122	12.7%
	Heave	115.325	40,980.4	0.081135	0.00277	0.179	26.7%
	Pitch	4208.76	10,625,100	0.022269	6.11e-05	9.39e-04	19.3%

Table 4: *LoCO PID Controller Gains and Characteristics*

Similar trends are seen with the PID controller as was seen with the PI controller in the areas of the proportional and integral gains, as well as with the rise and settling times. One area of difference lies with the derivative control gain. The tuner used did not provide any derivative control gain for any of the surge or yaw motions at any of the velocities. With that, it did modify the proportional and integral gains so that there was no oscillation about the steady state value but settled down to it after reaching the maximum overshoot point. In that same line, the values of the maximum overshoots decreased, nearly by half in the case of surge movement. This is critical for situations where fine control is required like when working near wildlife or divers.

Like with the PI controllers, each of the controllers detailed in Table 4 is a stable controller that uses feedback to reach the desired steady state value. While the proportional and integral gains at the highest velocity are not nearly as high as they are for the PI controller, they are on the same order and still unreasonably high. This is again attributed to some potentially erroneous hydrodynamic and added mass values upon which the motion in the vertical *xz*-plane relies on.

4.4. Conclusion

This section examined critical control characteristics and their relevancy to control systems. Additionally, PID control systems were defined and the inter-relations of their gains were examined to better understand how implementing parts of a PID system have an effect on the overall system performance. Finally, PI and PID control systems

were designed specifically for the LoCO transfer equations. From looking at the performance of the PI and PID systems, as well as what qualities it is vital for LoCO to have, the PID system seems to be a better fit without being able to perform any amount of real world testing due to the Coronavirus pandemic.

Chapter 5

Conclusion

The goal of this thesis has been to design an automatic control system capable of autonomous navigation and minimal human interaction when provided with a defined path.

5.1. Review

In an attempt to design an automatic control system for LoCO AUV, this thesis has examined the mathematical modeling of rigid underwater vehicles in 6 DOF and reduced the 6 DOF model to two, 3 DOF models based on LoCO's specific capabilities. The two systems developed are in the horizontal and vertical *xz*-planes motion. Both of the systems were linearized about a specific, forward velocity, the stabilities of each system was analyzed, and the transfer functions needed to control in each direction of motion was determined. Beyond that, PI and PID controllers were designed using MATLAB and the control characteristics of each, relative to the direction of motion and linearized velocity, has been analyzed.

5.2. Conclusions

Based on this analysis, the two systems of equations needed to define LoCO's motion have been determined. These systems are the basis upon which any control systems for LoCO, including the ones designed herein, can be built. Additionally, it has been determined that the PID controllers designed for LoCO are likely the best initial controllers to be implemented on the AUV given their ability to stabilize the system and due to their slightly better performance characteristics over the PI controller. This

decision has been made specifically with LoCO in mind since minimization of oscillations and maximum overshoot is critical for the video work and human-robot interaction capabilities required for this platform.

5.3. Recommendations for Future Work

Future work should include in-person experimental analyses performed with the control system designed herein. If possible, it would have been ideal to be able to experiment with variations in robustness vs. aggressiveness in the control system design and get feedback from LoCO users on what their preferences are. Additionally, depending on how well the vehicle controls, it is possible that additional stability from the system will be desired. In this case, a stability augmentation system (SAS) can be put in place alongside the designed PID controller. A SAS would be a separate controller designed with the intent to minimize oscillatory motions due to disturbances, while the controller already in place would control with the intent of achieving a goal. Beyond that, different types of variable control systems can be experimented with that would have been too technically difficult for the author to implement in this first iteration of the control system. The hope for this control system is that it provides a foundation for more advanced LoCO control systems and can provide enough information to those interested in learning about or tuning the LoCO control system to do so.

References

[1] NOAA, “What is the difference between an AUV and an ROV?,” 2021. https://oceanservice.noaa.gov/facts/auv-rov.html#:~:text=AUV stands for autonomous underwater,for commercial and recreational vessels.

[2] G. B. Skomal, E. M. Hoyos-Padilla, A. Kukulya, and R. Stokey, “Subsurface observations of white shark Carcharodon carcharias predatory behaviour using an autonomous underwater vehicle,” *J. Fish Biol.*, vol. 87, no. 6, pp. 1293–1312, 2015, doi: 10.1111.

[3] S. M. Smith *et al.*, “Results of an experiment using AUVs for shallow-water mine reconnaissance,” 1999, [Online]. Available: https://www-spiedigitallibrary-org.ezp1.lib.umn.edu/conference-proceedings-of-spie/3711/1/Results-of-an-experiment-using-AUVs-for-shallow-water-mine/10.1117/12.354651.full?SSO=1&tab=ArticleLink.

[4] F. J. Gutierrez, M. Gutowski, S. Ganther, P. Hogarth, and C. Wallace, “Deep rippled bedforms in Loch Ness: Evidence from an AUV bathymetry survey,” 2014, doi: 10.1109/AUV.2014.7054406.

[5] J. Chun-meng, W. Lei, and S. Yu-shan, “Design of motion control system of pipeline detection AUV,” *J. Cent. South Univ.*, vol. 24, no. 3, pp. 637–646, 2017, doi: 10.1007/s11771-017-3464-2.

[6] G. Bo, R. E. Randall, and K. E. Albaugh, “In select applications, AUVs work faster, cheaper than tethered vehicles,” *Offshore*, 2002. https://www.offshore-

mag.com/subsea/article/16759928/in-select-applications-auvs-work-faster-cheaper-than-tethered-vehicles (accessed Dec. 04, 2021).

[7] J. Yuh, “Design and Control of Autonomous Underwater Robots: A Survey.” Kluwer Academic Publishers, 2000, [Online]. Available: https://citeseerx.ist.psu.edu/viewdoc/download?doi=10.1.1.407.2159&rep=rep1&type=pdf.

[8] R. K. Lea, R. Allen, and S. L. Merry, “A comparative study of control techniques for an underwater flight vehicle,” *Int. J. Syst. Sci.*, vol. 30, no. 9, pp. 947–964, 1999, [Online]. Available: http://www.focus-offshore.com/Docs/ControlTechniques.pdf.

[9] C. Edge *et al.*, “Design and Experiments with LoCO AUV: A Low Cost Open-Source Autonomous Underwater Vehicle,” 2020. [Online]. Available: https://arxiv.org/pdf/2003.09041.pdf.

[10] O. M. Y. Chiu, “A Stability and Control System for a Hexapod Underwater Robot,” McGill University, 2008.

[11] P. Giguere, Y. Girdhar, and G. Dudek, “Wide-Speed Autopilot System for a Swimming Hexapod Robot,” 2013, doi: 10.1109/CRV.2013.13.

[12] T. Fossen, *Guidance and Control of Ocean Vehicles*. John Wiley & Sons, 1994.

[13] S. Wadoo and P. Kachroo, *Autonomous Underwater Vehicles: Modeling, Control Design, and Simulation*, 1st ed. Taylor and Francis Group, LLC, 2011.

[14] J. Gonzalez Agudelo, “Contribution to the Model and Navigation Control of an Autonomous Underwater Vehicle,” Universitat Politecnica de Catalunya, 2015.

[15] SNAME, “Nomenclature for Treating the Motion of a Submerged Body Through a

Fluid," New York, 1950. [Online]. Available: https://www.itk.ntnu.no/fag/TTK4190/papers/Sname 1950.PDF.

[16] K. Orpen, "Dynamics Modeling and Simulation of an Autonomous Underwater Vehicle (AUV)," University of Minnesota - Twin Cities, 2021.